Supporting Information

van Zanten et al. 10.1073/pnas.1003876107

SI Text

SI Materials and Methods. ***Antibody staining.*** THP-1 monocytes or DCs were allowed to adhere on poly-L-lysine (PLL) coated coverslips for 45 min at 37 °C. After blocking with I-buffer (PBS containing 3% BSA and 20 mM Glycine) for 30 min on ice, cells were labeled with ice-cold 10 μg/mL CTxB conjugated to Alexa 647 for 30 min on ice to prevent CTxB internalization. Negligible internalization was confirmed by double labeling CTxB extracellularly with fluorescent anti-CTxB Ab. After washing with ice-cold PBS, cells were fixed using 1% PFA in PBS for 20 min, followed by PBS washing steps and again blocking with I-buffer (containing 2% human serum) for 1 h. The proteins of interest were then labeled with either 10 μg/mL anti-LFA-1 (mAb TS2/4, kindly provided by E. Martz) anti-CD55 (143-30 from CLB) or anti-CD71 (clone B3/25 from SALK, DCB Trowbridge). Secondary Ab staining was performed with Alexa 488-conjugated goat antimouse IgG. Finally, the samples were washed with PBS and stored in PBS containing 1% PFA until use.

Commentary on fixation conditions using PFA (1–2%). In our experiments we have used mild cell fixation with 1–2% PFA to minimize the risk of artificial clustering and minimally disturb the cell membrane as demonstrated by previous work from our group (1–4). Briefly, receptor clustering is not artificially enhanced upon PFA fixation because similar sample preparations render different results in terms of aggregation on the cell membrane: receptors such as DC-SIGN on intermediate dendritic cells, CD71 and GPI-APs on monocytes organize in a monomeric fashion, whereas DC-SIGN on immature dendritic cells and LFA-1 on monocytes organize in nanoclusters (1–6). Furthermore, cell membrane morphology remains unperturbed as directly observed from high-resolution atomic force microscopy, shear-force imaging and TEM (1–6).

Cholesterol depletion experiments. To verify that the specific organization of CTxB tightened GM1 is cholesterol dependent we treated the cells with MβCD according to the following procedure: Approximately 2×10^5 cells, resuspended in serum-free RPMI medium 1640, were allowed to stretch onto PLL-coated coverslips at 37 °C. After stable attachment, cells were treated with 10 mM MβCD for 30 min at 37 °C under serum-free conditions. All subsequent solutions contained 10 mM MβCD to prevent reinsertion of cholesterol. After washing with ice-cold PBS, cells were blocked with PBS containing 3% fatty-acid free BSA for 30 min and then stained with CTxB (10 μg/mL) for another additional 30 min. After washing with ice-cold PBS, cells were fixed using 1% PFA in PBS for 20 min and stored in 1% PFA at 4 °C until analysis by NSOM.

NSOM imaging on MβCD-treated samples was performed on smaller areas, typically (3×3) and (4×4) μm^2, and at low scanning speeds (~2 μm/s) to minimally perturb the samples with the NSOM probe. In these conditions, sensitivity and spatial resolution are not compromised as demonstrated by the quantitative data analysis of spots sizes shown in Fig. S3. Moreover, to confirm that the fixation process by PFA effectively worked on MβCD-treated samples, we performed single particle tracking experiments of individual CTxB-GM1 on fixed MβCD-treated cells. The results are shown in Fig. S4*F* and confirm complete immobilization of CTxB-GM1 under these conditions.

Determination of the number of dyes per CTxB molecule. The number of CTxB molecules contained in each domain is directly related to the domain fluorescence intensity. However, to quantify its intensity it is necessary to determine first the intensity of individual CTxB labeled with the dye Alexa 647, i.e., to determine the number of dyes attached to each CTxB molecule and the labeling variability. To that end we recorded first the intensity as a function of time for multiple individual CTxB-Alexa 647 molecules bound to glass coverslips. This was achieved by placing the excitation light (1 kW/cm^2) above each isolated CTxB spot on glass, and monitoring the fluorescence emission in time. A typical recording from an individual CTxB molecule is shown in Fig. S1*A*, *Left*. The time trace exhibits different intensity levels, consistent with the presence of multiple Alexa 647 dyes per CTxB (6 dyes in this particular example). The last intensity step corresponds to the intensity of an individual Alexa 647 dye. Over 35 traces, normalized to an excitation intensity of 1 kW/cm^2, we find an average intensity of 1.8 ± 0.1 kcounts/s (with a FWHM of 1 kcounts/s) for this last step; i.e., the photon emission of a single Alexa 647 dye. We then related the average intensity of this last step to the average intensity of the highest step on each of the time traces. This results in ~8 dyes per CTxB molecule with a standard deviation of ~5 dyes per CTxB, which is in reasonable good agreement with the manufacturer specification (Molecular Probes) of 5–10 dyes per CTxB.

Simulations of random surface organization to assess the degree of real CTxB-GM1 clustering. To estimate the random probability of apparent clustering caused by the stochastic overlap of nearest neighbor signals we have generated in silico fluorescence images with a random particle organization using the experimental parameters, and quantified the brightness of the resulting individual spots. The resulting distributions were then compared with the experimental data. Any deviation from the simulated distribution of random organization reveals the degree of true clustering.

"Random fluorescence distribution images" were generated using a custom-written Labview program. The simulation places particles at random positions in a 2D area similar in size to the experimental optical image. The adjustable parameters in the program are: image area, A (in μm^2); number of pixels in the image; particle density, D (in particles/μm^2); particle intensity, I (in counts); standard deviation of particle intensity, I_d (in counts) and image resolution given by the aperture of the NSOM probe, R (in nm). D is obtained from the experimental spot density on the images together with the experimentally obtained intensity distributions shown in Fig. 2*G*. In the case of the glass substrate (Fig. S1*B*) the simulations have been performed with $D = 10$ particles/μm^2 and for simulations shown in Fig. S1*C* (cell membrane) with $D = 100$ particles/μm^2. This density has been obtained as follows: the spot density has been extracted directly from the images rendering a value of (4.8 ± 0.7) spots/μm^2. The intensity distributions are shown in Fig. 2*G*. To obtain the number of CTxB molecules per spot we divide the main distribution by the intensity distribution obtained on glass and corresponding to individual CTxB molecules. This results in a distribution of CTxB per spot with a peak at ~6 CTxB molecules, and a longer tail up to ~20 CTxB molecules per spot. Thus, the surface density of CTxB molecules varied from ~30 molecules/μm^2 up to ~100 molecules/μm^2. Given this broad surface density we performed the simulations considering the upper surface density; i.e., $D = 100$ molecules/μm^2 so that the simulated results provide the maximum number of possible random coincidence events.

During the simulation, A and D are used to calculate the total number of particles that will be distributed in A. The (x, y) coor-

dinates of each individual particle are obtained from a random number generator. In this way, particles with the size of a single pixel are randomly distributed in the simulated image areas. To include the effect of a limited optical resolution, the pixels are convoluted with a 2D Gaussian with a FWHM that is equal to the resolution settings. The spot intensity distributions were obtained through analysis of the simulated fluorescence images by a custom-written Labview analysis program. Briefly, a spot is defined using a circle of radius r, where r is chosen such that the spot diameter corresponds to the image resolution. The average spot intensity is obtained by adding all pixel intensities within r and dividing by the total number of pixels in r. The number of particles in the spot is then obtained by dividing the average spot intensity by the average intensity of a single CTxB. The results of the simulations and experimental data for CTxB on glass and CTxB-GM1 on monocytes are shown in Fig. S1 *B* and *C* respectively.

As observed in Fig. S1*B*, the simulated image (*Left*) and the experimentally obtained image (*Center*) on the glass substrate agree exceedingly well with each other as also reflected by the distribution of particles per fluorescence spot on both simulated and experimental data (*Right*). Thus, the occurrence of small CTxB nanoaggregates on the glass is due to the random occurrence of nearby CTxB molecules and do not reflect true clustering. Importantly, the variability on the intensity per spot (I_d) arising from the variation on the number of dyes per CTxB has been important to correctly reproduce the experimentally obtained fluorescence images. On the contrary, the results on the cell membrane (Fig. S1*C*) show clear differences between simulated (*Left*) and experimental data (*Center*), with the distribution of the experimental data being significantly shifted toward higher number of particles per spot compared to the simulated data (*Right*). Furthermore, the experimental distribution has very few occurrences for low number of particles per spot, indicating that most of the CTxB-GM1 molecules are incorporated in small clusters. Thus, these data indicate that whereas the random coincidence of nearby signals would result in apparent small nanoaggregates on the cell membrane, the experimental data show much larger degree of CTxB-GM1 aggregation beyond that of stochastic coincidence confirming the organization of CTxB-GM1 as real nanodomains on the cell surface.

Experimental spot densities. The results shown in Fig. 3 *B–D* correspond to 282 occurrences for CD55:GM1 (282 CD55 and 1106 CTxB-GM1 spots); 420 occurrences for LFA-1:GM1 (420 LFA-1 and 880 CTxB-GM1 spots) and 511 occurrences for CD71:GM1 (511 CD71 and 430 CTxB-GM1 spots), obtained over multiple NSOM images from different cells. Random simulations of i-nnd were performed by using the spot densities as derived from multiple images (CD55 = 1.4 spots/μm^2 and CTxB-GM1 = 5.6 spots/μm^2; CD71 = 5.1 spots/μm^2 and CTxB-GM1 = 4.3 spots/μm^2; and LFA-1 = 2.1 spots/μm^2 and CTxB-GM1 = 4.5 spots/μm^2), and placing both protein and CTxB-GM1 spots at random (x, y) positions. Nearest interdomain distances between the random (x, y) positions of proteins and the random nearest neighbor CTxB-GM1 (x, y) positions were calculated in the same way as for the experimental data.

Fluorescence recovery after photobleaching (FRAP) experiments. To assess the degree of diffusion after cell fixation, we performed FRAP measurements over multiple cells fixed with 1% PFA. Experiments were performed on a Zeiss LSM 510 microscope using a PlanApochromatic 63 × 1.4 oil immersion DIC objective and with the confocal pinhole fully open. Fixed cells were labeled following the procedure reported above for the NSOM samples. Photobleaching of Alexa647 was performed using repeated scans with the 633 nm laser line at full power over an area of 3 × 3 μm^2. Pre- and postbleached images were monitored at low laser intensity. Fluorescence recoveries in the bleached region were quantified using Zeiss LSM Image Browser version 3.2. Recovery curves were averaged over multiple cells for CTxB-GM1 in fixed cells and CTxB-GM1 in living cells at 20 °C.

The results shown in Fig. S4*A* on unfixed, living cells at 20 °C show recovery curves up to 50% (blue curve) consistent with previous reports where lack of full CTxB recovery has also been observed (7, 8). In the case of fixed cells, a minor 10% of mobile CTxB-GM1 is found (red and black curves). We have assessed from the FRAP curves the residual mobility of this small fraction of molecules using the relation $I_t = I_f\sqrt{1-\frac{\omega^2}{\omega^2+4Dt\pi}}$ where I_t is the intensity as function of time, I_f is the intensity after recovery, ω is the width of the bleached area (3 μm in our case) and D is the one-dimensional diffusion constant. From the FRAP curves, this 10% of residual mobile molecules after PFA fixation have a very small diffusion value ($D < 0.005$ $\mu m^2/s$). Clearly, this mobility is not due to unbound CTxB, which would move much faster. Most probably, these values correspond to inaccuracies of the method to determine such small D values and thus the difficulty to discriminate slow from immobile molecules using FRAP.

Single particle tracking experiments to assess the mobility of CTxB-GM1 at 4 °C and after PFA-fixation. To confirm complete fixation of CTxB-GM1 on fixed cells treated with 1–2% PFA, we followed the lateral mobility of individual CTxB-GM1 using a single molecule epifluorescence microscope. Samples were prepared as follows:

CTxB-GM1 labeling. THP-1 cells were allowed to adhere to PLL-coated coverslips following the same procedure as described above. CTxB binding to GM1 was performed as described for NSOM analysis, except that CTxB was used at a final concentration of 0.005 μg/mL and CTxB incubation time was 3 min. Three sets of samples were investigated with the single molecule setup: (*i*) unfixed cells after incubation at 4 °C; (*ii*) fixed cells (1–2% PFA) after CTxB incubation at 4 °C; and (*iii*) MβCD-treated cells, fixed (1–2% PFA) after CTxB incubation at 4 °C.

Single molecule epifluorescence microscopy. Experiments were performed on a home-built setup. Samples were illuminated for 5 ms at 633 nm by a HeNe laser and images recorded at a frame rate of 10 Hz. A defocusing lens allowed illumination of a 27 μm^2 area with an excitation intensity of 1.35 kW/cm^2. Fluorescence was collected with a 1.45 NA oil immersion objective and guided to an intensified CCD camera (IPentamax, Princeton Instruments) through appropriate filters.

Fluorescence trajectories analysis. Two-dimensional trajectories of individual CTxB fluorescent spots in the focal plane were reconstructed using custom made software based on Matlab. Only trajectories containing at least thirteen points were retained for further analysis. Mean square displacements (MSD) versus time lag (t_{lag}) plots were generated for all possible t_{lag} intervals throughout each trajectory. The slope of the first four points in the MSD plots was determined and the relationship MSD = $4Dt_{lag}$ was used to derive the short-range diffusion coefficient D. Localization accuracy on the determination of the (x, y) coordinates for generating single molecule trajectories was 30–40 nm in our experimental conditions. The precision on the determination of D (fitting of the first four points to the MSD plots) also depends on the trajectory length. For trajectories of thirteen points like the ones used for our analysis (limited by photobleaching) the minimum detectable D value is 0.006 $\mu m^2/s$, with 95% confidence level; i.e., trajectories with $D < 0.006$ $\mu m^2/s$ under our experimental conditions are considered as immobile. The results are shown in Fig. S4 *B–F* for the three samples investigated and

demonstrates full immobilization of CTxB-GM1 in all conditions investigated.

Monte Carlo simulations. A two-dimensional lattice discretized in 1024×1024 sites was used to represent a cell membrane. A lattice site has a surface of $5\ \text{nm} \times 5\ \text{nm}$, for a total simulated membrane surface of $26.21\ \mu\text{m}^2$. Each site can be occupied by raft-like lipids, non-raft-like lipids or a protein particle. Raft-like lipids are assumed to occupy the 25% of the total membrane area, organized in nonoverlapping circular regions of radius R. The units of CTxB-GM1 are fixed to single sites in the raft-like regions. Additionally, the lattice is seeded with a number of diffusing proteins. Affinity of these proteins to raft-like regions is introduced by lowering the energy of the system with an amount J (in k_BT units) for each protein particle in contact with a raft-like site. A Monte Carlo algorithm is implemented to move the proteins: a protein particle is selected and a new location is chosen at random. The energy variation ΔE of the attempted move is computed and determines an exchange probability $p = \exp(-\Delta E/k_BT)$. The acceptance of the move is based on the Metropolis algorithm: if $p > 1$, the move is accepted; if $p < 1$, a random number, ζ, uniformly distributed between 0 and 1, is generated, and the move is accepted if $p > \zeta$. This process is repeatedly applied up to equilibration. The proposed Monte Carlo method does not reproduce the realistic kinetics of the system because real diffusion occurs by exchange of nearest neighbor particles, but it ensures the fastest equilibration and has no effect on the equilibrium properties of the system.

Direct comparison of MC simulations to NSOM images. To allow direct comparison with the experimental results, particle distributions from simulations are converted into intensity images according to a given resolution, mimicking the effect of the probe used in the experiments. First, the effect of optical resolution is included by convoluting each image pixel with a 2D Gaussian function with a FWHM equal to the resolution setting of the NSOM tip radius. Second, using a curvature criterion, spot domains are identified in the convoluted images. Finally, the centers of mass of each of these spots are determined and the interdomain distance distributions are computed. Notice that after image processing some initial inserted particles (CTxB-GM1 units or protein particles) are convoluted into a single spot. Therefore, to reproduce a given spot density, a larger number of initial particles had to be used in the simulation.

1. Koopman M, de Bakker BI, Garcia-Parajo MF, van Hulst NF (2003) Shear force imaging of soft samples in liquid using a diving bell concept. *Appl Phys Lett* 83:5083–5085.
2. Koopman M, et al. (2004) Near-field scanning optical microscopy in liquid for high-resolution single molecule detection on dendritic cells. *FEBS Lett* 573:6–10.
3. de Bakker BI, et al. (2007) Nanoscale organization of the pathogen receptor DC-SIGN mapped by single-molecule high-resolution fluorescence microscopy. *ChemPhysChem* 8:1473–1480.
4. van Zanten TS, et al. (2009) Hotspots of GPI-anchored proteins and integrin nanoclusters function as nucleation sites for cell adhesion. *Proc Natl Acad Sci USA* 106:18557–18562.
5. Cambi A, et al. (2004) Microdomains of the C-type lectin DC-SIGN are portals for virus entry into dendritic cells. *J Cell Bio* 164:145–155.
6. Cambi A, et al. (2006) Organization of the integrin LFA-1 in nanoclusters regulates its activity. *Mol Biol Cell* 17:4270–4281.
7. Kenworthy AK, et al. (2004) Dynamics of putative raft-associated proteins at the cell surface. *J Cell Biol* 165:735–746.
8. Bacia K, Scherfeld D, Kahya N, Schwille P (2004) Fluorescence correlation spectroscopy relates rafts in model and native membranes. *Biophys J* 87:1034–1043.

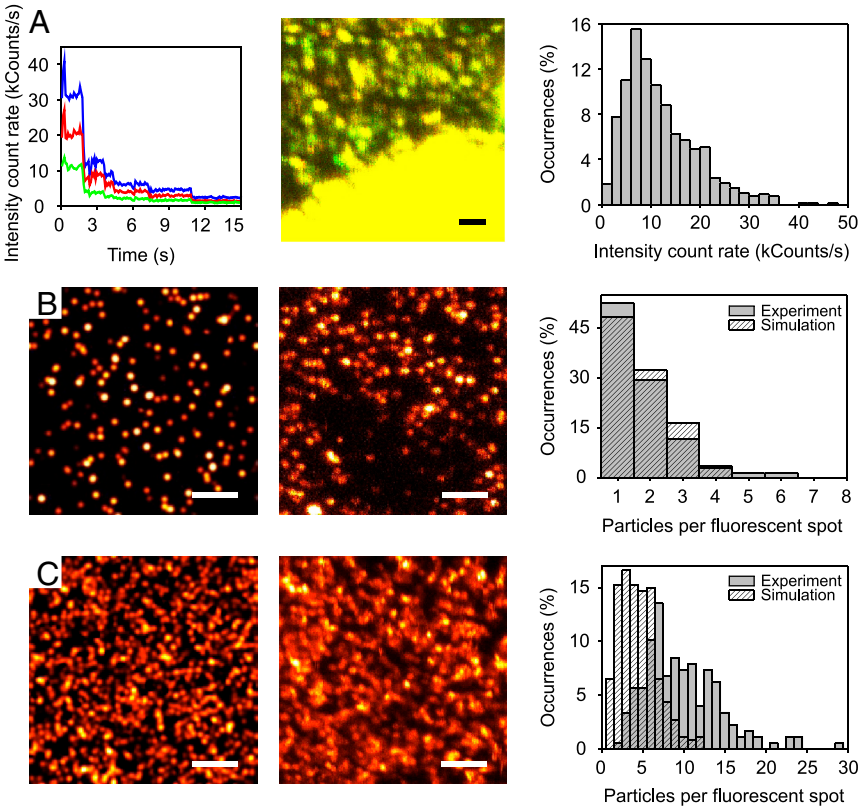

Fig. S1. Quantification of the intensity of individual CTxB spots on glass and simulations to assess the degree of apparent clustering of CTxB labeled with Alexa 647 due to high packing density and NSOM resolution on glass and on the cell membrane. (*A*) (*Left*) Fluorescence intensity as a function of time recorded on a CTxB-Alexa647 isolated spot on glass using polarization sensitive detection (red and green for the independent channels and blue for the total signal) with an excitation intensity of 1 kW/cm^2. The multiple step behavior is characteristic of several fluorescence dyes (6 in this particular example) attached to one CTxB. (*Center*) NSOM image of a region of the sample containing part of the cell membrane (bright lower part) and the glass substrate (upper part). Brightness on the image has been intentionally adjusted such as to visualize CTxB spots on the glass next to the cell regions. (*Right*) Quantification of the spot brightness obtained from individual CTxB spots nonspecifically attached to the glass next to the cells (677 spots on the glass surfaces from 7 independent NSOM images). Because different NSOM tips (90–110 nm in diameter) have been used for imaging resulting in different excitation intensities (~0.2–0.3 kW/cm^2), all the images were normalized with respect to the glass background intensity. The intensity distribution peaks at ~9 kcounts/s and has a tail toward higher intensity values. The extent of the tail is larger than the standard deviation obtained from the dye variability suggesting that there might be some small "apparent" aggregates on CTxB glass. (*B*) Simulated (*Left*) and experimentally obtained (*Center*) fluorescence images of CTxB distributed on the glass surface next to the cells. The simulated settings correspond to the experimental data with $D = 10$ particles/μm^2. (*Right*) Number of particles per fluorescent spot as derived from the experimental data (gray bars) together with simulations of random organization (dashed bars). The good agreement between experimental and simulated data indicates that the degree of apparent aggregation of CTxB observed on glass is not real but due to the random coincidence of close-by CTxB molecules. (*C*) Simulated (*Left*) and experimentally obtained (*Center*) fluorescence images of CTxB-GM1 on monocytes. The simulated settings correspond to the experimental data with $D = 100$ particles/μm^2. (*Right*) Number of particles per fluorescent spot as derived from the experimental data (gray bars) together with simulations of random organization (dashed bars). The large deviation between simulated and experimental data demonstrates that the CTxB-GM1 nanodomains on the cell surface are real and not resulting from the random occurrence of nearby molecules.

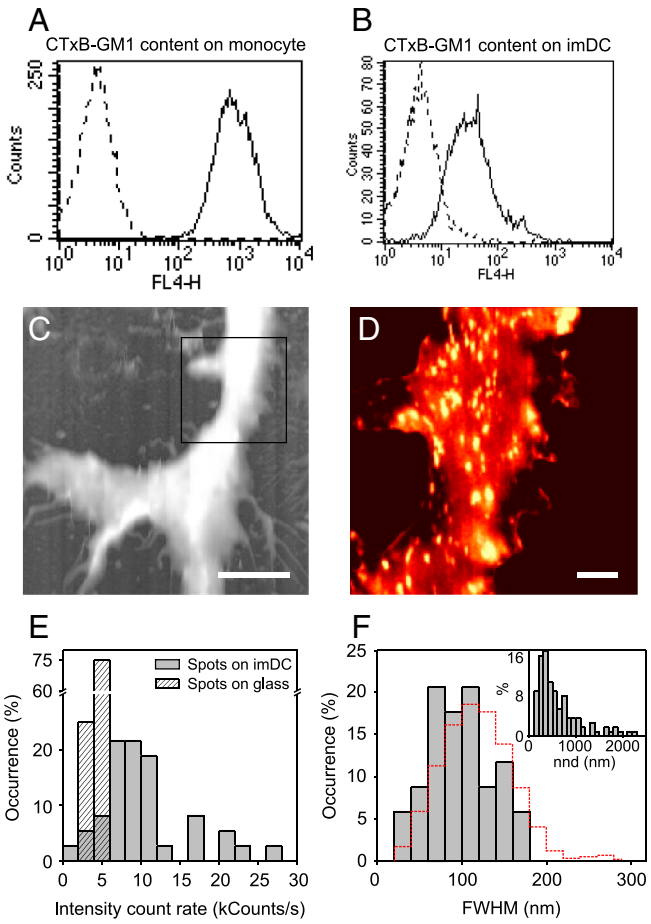

Fig. S2. CTxB-GM1 organizes in nanodomains on immature dendritic cells (imDC), despite its lower expression as compared to monocytes. (*A*, *B*) Expression levels of GM1 as determined by flow cytometry on monocytes (*A*) and imDCs (*B*). The dotted line represents the background fluorescence arising from unstained cells, and the continuous line indicates the specific CTxB-GM1 stained distribution. (*C*) Topography obtained from an imDC using shear-force NSOM. Scale bar: 5 μm. (*D*) High-resolution NSOM image of CTxB-GM1 nanodomains of the highlighted area in C. Scale bar: 1 μm. (*E*) Intensity distribution histogram obtained for CTxB-GM1 nanodomains on imDC (gray bars) and compared to individual CTxB molecules on glass (dashed bars). The longer tail of the intensity distribution on imDCs compared to glass confirms nanodomain organization of CTxB-GM1 on imDCs. (*F*) Histogram of the distribution of full-width-half-maximum (FWHM) of individual CTxB-GM1 nanodomains over multiple cells (gray bars) and of scarcely found individual CTxBs on the glass (dotted red line) in the same experiment. Inset displays the nearest neighbor distribution (nnd) of the CTxB-GM1 spots on intact imDCs with a characteristic interdomain separation of ~400 nm.

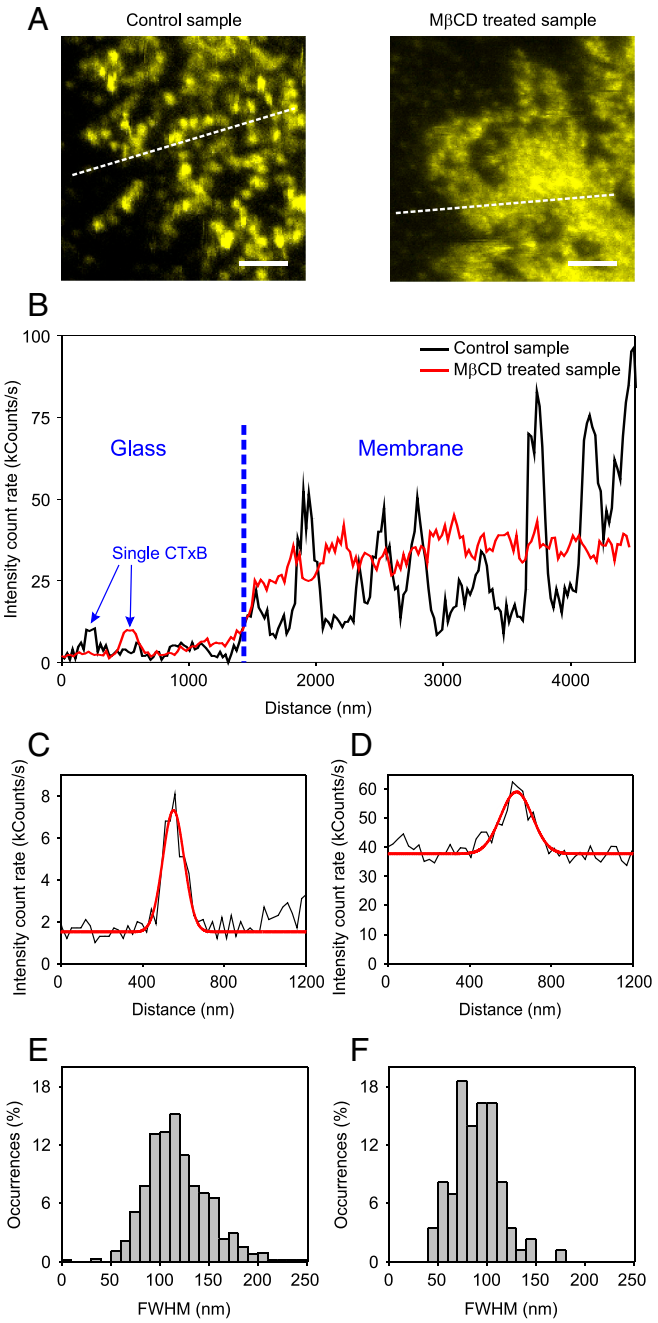

Fig. S3. Cholesterol depletion significantly affects the nanometer-scale ordering of CTxB-GM1 on the cell membrane. (*A*) Representative NSOM images of CTxB-GM1 nanodomains on an untreated sample (*Left*) and after cholesterol depletion with MβCD (*Right*). Scale bars: 1 μm. (*B*) Intensity profiles (intensity versus distance) of the untreated cell (black line) and MβCD-treated cell (red line) taken along the dashed white lines drawn on images shown in A. Note that although the background fluorescence above the glass (left side of the plots) is similar for both profiles and showing single molecule features of comparable intensity, the large intensity peaks arising from the CTxB-GM1 nanodomains on the untreated cell strongly contrast with the more irregular intensity profile from the MβCD-treated cell suggesting a significant dispersion of CTxB-GM1 nanoclusters after cholesterol depletion. (*C*) Single CTxB spot profile on glass next to the MβCD-treated cells with FWHM ~100 nm and (*D*) Intensity line profile of a fluorescent feature on the cell membrane above the higher continuous background. (*E*) Spot size distribution of CTxB on glass for the untreated sample and (*F*) similar distribution for the MβCD-treated samples. The results shown in C-F demonstrate that NSOM resolution and sensitivity are equal on untreated and MβCD-treated cells, ruling out the possibility that the more uniform fluorescence obtained on MβCD-treated cells is due to a decrease of spatial resolution arising from a change of elasticity of the membrane after cholesterol depletion.

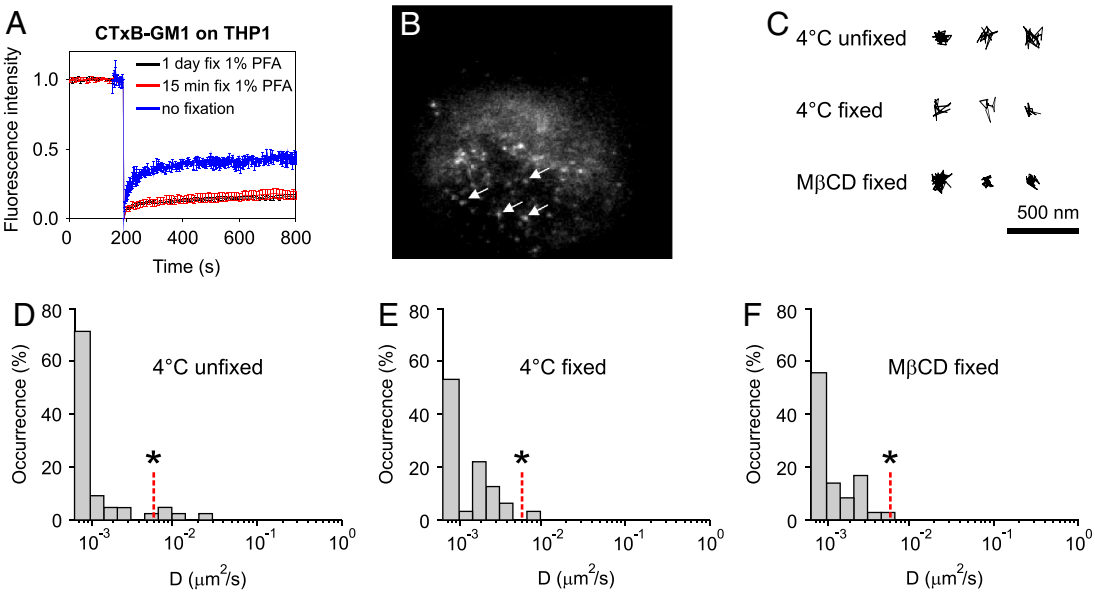

Fig. S4. True nanometer-scale colocalization by NSOM leads to a high *C* value and "nearest interdomain distances" concentrated around zero. To confirm that true colocalization indeed leads to high *C* values and interdomain distances different from the ones shown in Fig. 3 *B* and *C*, we performed dual-color NSOM imaging on the receptor CD71 after labeling with the primary antibody anti-CD71 conjugated to Alexa 647 (*A*) and the secondary antibody goat antimouse IgG conjugated to Alexa 488 (*B*). Scale bars: 1 μm. As expected, images in (*A*) and (*B*) are essentially identical in terms of spatial patterning, consistent with the fact that both primary and secondary antibodies map the same receptor on the cell surface. (*C*) Overlapping of both (*A*) and (*B*) shows a high degree of colocalization, as indicated by the large occurrence of yellow spots and the high colocalization coefficient *C* obtained ($C = 0.75 \pm 0.07$) from 3 different NSOM images analyzed. (*D*) Nearest neighbor distance analysis between "red" and "green" spots (bars) together with simulations of random spatial distribution of "red" and "green" spots at the experimental spot densities. The concentration of all occurrences close to zero indicates true colocalization between the two labels. The inset shows the nnd distribution concentrated around ~13 nm. Because the localization accuracy in the images is $\sigma \sim 5$ nm, this value most probably reflects the effective distance between both dyes, which are separated by the length of the secondary antibody (1).

1 Pease LF, et al. (2008) Determination of protein aggregation with differential mobility analysis: Application to IgG antibodies. *Biotechnol Bioeng* 101:1214–1222.

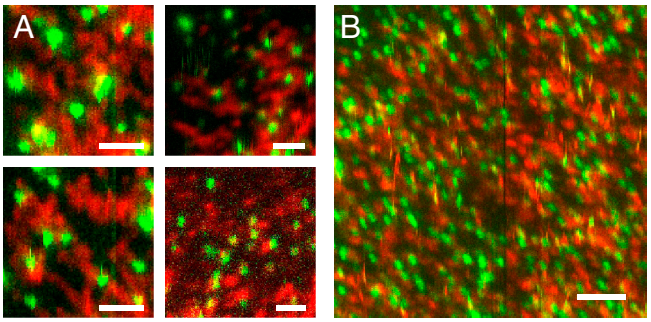

Fig. S5. FRAP and SPT experiments confirm complete immobilization of CTxB-GM1 nanodomains after PFA fixation. (*A*) Recovery curves of CTxB-GM1 on monocytes: 1 day after fixation (black line), 15 minutes after fixation (red line), and live cell on PLL (blue line). Each curve shows the mean ± SD calculated from several cells from two separate experiments. (*B*) Representative single molecule epifluorescence image obtained on the upper part of a monocyte membrane. Individual fluorescent spots correspond to single CTxB-GM1 nanodomains on the membrane. (*C*) Representative individual CTxB-GM1 trajectories obtained on unfixed cells labeled at 4 °C, cells labeled at 4 °C and fixed with 1% PFA, and MβCD-treated cells, labeled at 4 °C and fixed with 1% PFA. Visual inspection of the recorded trajectories shows that CTxB-GM1 nanodomains are immobile, irrespectively of the preparation conditions. (*D*) Distribution of the short-range diffusion coefficients obtained for 45 individual trajectories recorded on unfixed cells, (*E*) 45 individual trajectories recorded on fixed cells with PFA after CTxB labeling and (*F*) 36 individual trajectories from MβCD-treated cells, labeled at 4 °C and fixed. * denotes the accuracy threshold on the discrimination of immobile trajectories (given by the localization accuracy of the setup and trajectory length). The fraction of molecules showing residual mobility; i.e., above * is 9.5% in (*D*), 3.2% in (*E*) and 0% in (*F*).

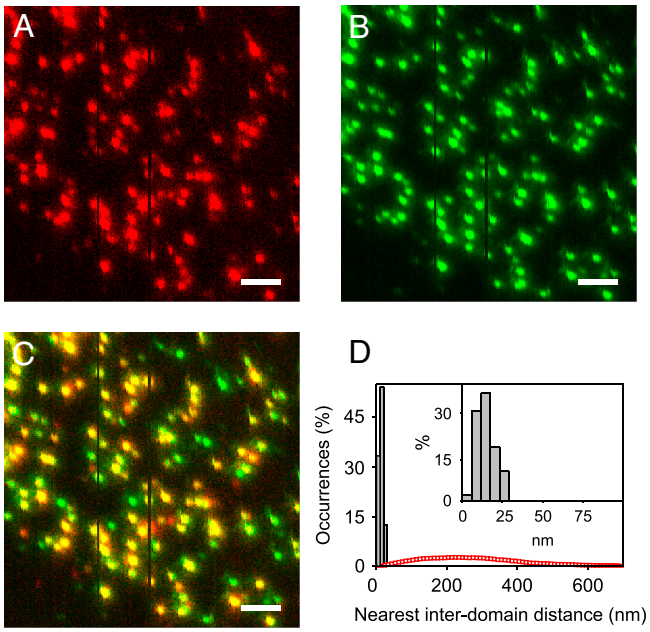

Fig. S6. Representative dual-color NSOM images. (*A*) LFA-1 (green) and CTxB-GM1 nanodomains (red). (*B*) CD71 (green) and CTxB-GM1 nanodomains (red). Due to the large extracellular region of LFA-1 (>30 nm) (1), NSOM imaging had to be performed on smaller regions of the cell membrane to minimize dragging of these molecules while scanning. Images shown in (*A*) correspond thus to smaller areas of the membrane. Scale bars in (*A*): 500 nm. Scale bar in (*B*): 1 μm.

1 Qi SY, Groves JT, Chakraborty A (2001) Synaptic pattern formation during cellular recognition *Proc Natl Acad Sci USA* 98:6548–6553.

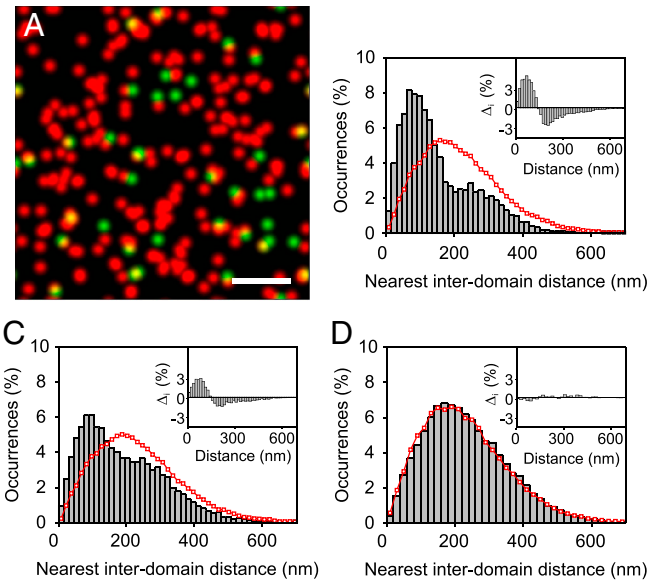

Fig. S7. In silico experiments. (*A*) Representative convoluted image obtained from the Monte Carlo simulation with protein and CTxB-GM1 nanodomain densities taken from experimental data of CD55 and CTxB-GM1. (*B–D*) Nearest interdomain distance distributions of (*B*) CD55, (*C*) LFA-1, (*D*) CD71 to its closest CTxB-GM1 nanodomain (gray bars) together with the case of random spatially distributed proteins and CTxB-GM1 nanodomains (red). The spot densities used for the simulations are identical to the ones obtained from the NSOM experiments. The radius of the raft-like regions, *R*, is assumed to be 100 nm and the protein affinities are $J = 2$ (B, CD55), $J = 1$ (C, LFA-1) and $J = 0$ (D, CD71). The insets correspond to the difference between the distribution obtained from the Monte Carlo simulations and the random distribution. The distributions are significantly different for *B* and *C* with $P = 0.004$, and similar for *D* with $P = 0.84$. Fitting of the short-distance distribution of the in silico data to a Gaussian function renders the characteristic size of the raft-like region, with peak values of 66 $(\sigma = 38)$ nm and 69 $(\sigma = 39)$ nm for CD55:CTxB-GM1 (*B*) and LFA-1:CTxB-GM1 (*C*) respectively.